JCI insight

Low-dose IL-2 selectively activates subsets of CD4$^+$ Tregs and NK cells

Masahiro Hirakawa, … , Robert J. Soiffer, Jerome Ritz

JCI Insight. 2016;1(18):e89278. https://doi.org/10.1172/jci.insight.89278.

Clinical Medicine | Immunology

CD4$^+$ regulatory T cells (CD4Tregs) play a critical role in the maintenance of immune tolerance and prevention of chronic graft-versus-host disease (GVHD) after allogeneic hematopoietic stem cell transplantation. IL-2 supports the proliferation and survival of CD4Tregs and previous studies have demonstrated that IL-2 induces selective expansion of CD4Tregs and improves clinical manifestations of chronic GVHD. However, mechanisms for selective activation of CD4Tregs and the effects of low-dose IL-2 on other immune cells are not well understood. Using mass cytometry, we demonstrate that low concentrations of IL-2 selectively induce STAT5 phosphorylation in Helios$^+$ CD4Tregs and CD56^{bright}CD16$^-$ NK cells in vitro. Preferential activation and expansion of Helios$^+$ CD4Tregs and CD56^{bright}CD16$^-$ NK cells was also demonstrated in patients with chronic GVHD receiving low-dose IL-2. With prolonged IL-2 treatment for 48 weeks, phenotypic changes were also observed in Helios$^-$ CD4Tregs. The effects of low-dose IL-2 therapy on conventional CD4$^+$ T cells and CD8$^+$ T cells were limited to increased expression of PD-1 on effector memory T cells. These studies reveal the selective effects of low-dose IL-2 therapy on Helios$^+$ CD4Tregs and CD56^{bright} NK cells that constitutively express high-affinity IL-2 receptors as well as the […]

JCI insight

RESEARCH ARTICLE

Low-dose IL-2 selectively activates subsets of CD4+ Tregs and NK cells

Masahiro Hirakawa,[1,2] Tiago R. Matos,[1,2,3] Hongye Liu,[1,2] John Koreth,[1,2] Haesook T. Kim,[4,5] Nicole E. Paul,[1] Kazuyuki Murase,[1,2] Jennifer Whangbo,[1,2,6] Ana C. Alho,[1,2,3] Sarah Nikiforow,[1,2] Corey Cutler,[1,2] Vincent T. Ho,[1,2] Philippe Armand,[1,2] Edwin P. Alyea,[1,2] Joseph H. Antin,[1,2] Bruce R. Blazar,[7] Joao F. Lacerda,[3] Robert J. Soiffer,[1,2] and Jerome Ritz[1,2]

[1]Division of Hematologic Malignancies and Department of Medical Oncology, Dana-Farber Cancer Institute, Boston, Massachusetts, USA. [2]Harvard Medical School, Boston, Massachusetts, USA. [3]Instituto de Medicina Molecular, Faculdade de Medicina, Universidade de Lisboa, Lisbon, Portugal. [4]Department of Biostatistics and Computational Biology, Dana-Farber Cancer Institute, Boston, Massachusetts, USA. [5]Harvard T. H. Chan School of Public Health, Boston, Massachusetts, USA. [6]Division of Hematology/Oncology, Boston Children's Hospital, Boston, Massachusetts, USA. [7]Division of Blood and Marrow Transplantation, University of Minnesota, Minneapolis, Minnesota, USA.

CD4+ regulatory T cells (CD4Tregs) play a critical role in the maintenance of immune tolerance and prevention of chronic graft-versus-host disease (GVHD) after allogeneic hematopoietic stem cell transplantation. IL-2 supports the proliferation and survival of CD4Tregs and previous studies have demonstrated that IL-2 induces selective expansion of CD4Tregs and improves clinical manifestations of chronic GVHD. However, mechanisms for selective activation of CD4Tregs and the effects of low-dose IL-2 on other immune cells are not well understood. Using mass cytometry, we demonstrate that low concentrations of IL-2 selectively induce STAT5 phosphorylation in Helios+ CD4Tregs and CD56^{bright}CD16^{-} NK cells in vitro. Preferential activation and expansion of Helios+ CD4Tregs and CD56^{bright}CD16^{-} NK cells was also demonstrated in patients with chronic GVHD receiving low-dose IL-2. With prolonged IL-2 treatment for 48 weeks, phenotypic changes were also observed in Helios^{-} CD4Tregs. The effects of low-dose IL-2 therapy on conventional CD4+ T cells and CD8+ T cells were limited to increased expression of PD-1 on effector memory T cells. These studies reveal the selective effects of low-dose IL-2 therapy on Helios+ CD4Tregs and CD56^{bright} NK cells that constitutively express high-affinity IL-2 receptors as well as the indirect effects of prolonged exposure to low concentrations of IL-2 in vivo.

Conflict of interest: John Koreth receives income from Amgen, Kadmon Corporation, and Takeda, and research support from Millennium, Otsuka, and Prometheus Laboratories. Philippe Armand receives research support from BMS, Merck, Tensha Therapeutics, and Roche. Jerome Ritz receives income from Biothera Pharmaceuticals and Delinia and research support from Merck, Nektar Therapeutics, Prometheus Laboratories, and Roche Oncology.
Bruce Blazer is listed as an inventor on a number of patents. For specific details see Supplemental Material.

Submitted: June 28, 2016
Accepted: September 26, 2016
Published: November 3, 2016

Reference information:
JCI Insight. 2016;1(18):e89278.
doi:10.1172/jci.insight.89278.

Introduction

Allogeneic hematopoietic stem cell transplantation (HSCT) is a potentially curative therapy for patients with various hematologic malignancies, immune deficiencies, and bone marrow failure syndromes. However, despite improved conditioning regimens, immunosuppressive therapies, and supportive care, chronic graft-versus-host disease (GVHD) remains a major complication of allogeneic HSCT and is the leading cause of long-term morbidity and mortality (1, 2). Advances in our understanding of chronic GVHD have established that both T and B cells, interacting in a highly complex network, contribute to tissue injury and the varied clinical manifestations of chronic GVHD (3, 4). Therapeutic approaches have relied primarily on broadly immune suppressive agents, with corticosteroids being the most effective standard therapy. B cell–directed therapies can also be effective but these also result in prolonged B cell depletion (5, 6).

CD4+ regulatory T cells (CD4Tregs), defined by expression of CD25 and FoxP3, play an indispensable role in the maintenance of self-tolerance and immune homeostasis (7, 8). Following allogeneic HSCT, thymic generation of CD4Tregs is markedly impaired and reconstitution of this critical T cell population is primarily driven by proliferation and expansion of mature memory CD4Tregs (9). Following transplant, rapidly proliferating CD4Tregs also exhibit increased susceptibility to Fas-mediated apoptosis (10) and increased mitochondrial apoptotic priming (11). Short telomeres and low levels of telomerase activity also contribute to reduced survival of CD4Tregs in vivo (12). Since these factors do not affect other T cell populations to the same extent, these factors all contribute to a relative deficiency of CD4Tregs compared with effector T cells and the subsequent development of chronic GVHD (9, 10).

To understand the functional heterogeneity of CD4Tregs and better define the differentiation of these cells in vivo, previous studies have examined expression of various cell surface and intracellular markers including CD45RA, HLA-DR, CD62L, FoxP3, RUNX, and Helios (13–18). Helios is an Ikaros-family transcription factor that was initially thought to be a marker of thymus-derived or natural CD4Tregs (18). However, other studies have shown that Helios is also expressed by induced CD4Tregs and that Helios expression is associated with activation, proliferation, and suppressive capacity of CD4Tregs (19–23). Taken together, these studies have established the considerable phenotypic and functional heterogeneity of CD4Tregs and provide a framework in which to further characterize the functional role of distinct CD4Treg subsets in disease settings and in response to therapeutic interventions.

IL-2 plays a critical role in the development, proliferation, functional activity, and survival of CD4Tregs (24–27). In contrast with effector T cells, CD4Tregs constitutively express high levels of CD25, forming a high-affinity receptor for IL-2. Since CD4Tregs cannot produce IL-2, these cells are inherently dependent on exogenous sources, predominantly activated effector T cells, for this critical homeostatic factor (28). However, because CD4Tregs express a high-affinity receptor, these cells respond to low concentrations of IL-2. Taking advantage of the sensitivity of CD4Tregs to IL-2, we have shown that daily administration of low-dose IL-2 in patients with active chronic GVHD results in sustained expansion of CD4Tregs without a significant increase in conventional $CD4^+$ T cells (CD4Tcons) or $CD8^+$ T cells and clinical improvement in more than 50% of patients with chronic GVHD (29, 30). Clinical trials at other centers have shown the selective effect of low-dose IL-2 therapy on CD4Tregs in healthy individuals, patients with hepatitis C virus–induced vasculitis, type 1 diabetes, acute GVHD, alopecia areata, and systemic lupus erythematosus (31–36). Laboratory studies have examined the mechanisms underlying the effects of IL-2 on CD4Tregs (37–39), but the effects of low-dose IL-2 on heterogeneous CD4Treg subsets and other lymphocyte populations remain poorly defined.

In the present study, we applied single-cell mass cytometry to dissect the effects of IL-2 on CD4Tregs, CD4Tcons, $CD8^+$ T cells, NK cells, and B cells in vitro. Mass cytometry allowed us to simultaneously measure expression of 33 proteins with single-cell resolution in multiple phenotypically and functionally defined subsets within each major lymphocyte population (40–42). Since our panel included markers of different cell signaling pathways as well as functional proteins and cell surface proteins, we were able to track intracellular signaling in response to IL-2 in each cellular subset. Finally, by comparing results of IL-2 stimulation in vitro with analysis of samples obtained from patients receiving low-dose IL-2 therapy, we were able to demonstrate that the therapeutic administration of exogenous low-dose IL-2 closely mirrored the effects of short-term stimulation with low concentrations of IL-2 in vitro. Thus, daily IL-2 therapy resulted in the selective activation and expansion of distinct subsets of $Helios^+$ CD4Tregs and $CD56^{bright}CD16^-$ NK cells without activation of CD4Tcons or $CD8^+$ T cells. With continued daily IL-2 treatment, these functional effects were maintained for prolonged periods up to 48 weeks.

Results

Definition of lymphocyte subsets in peripheral blood. Mass cytometry allowed us to simultaneously quantify expression of a large number of key functional markers in well-defined functional subsets of T, B, and NK cells in normal peripheral blood (Supplemental Table 1; supplemental material available online with this article; doi:10.1172/jci.insight.89278DS1). Major peripheral blood mononuclear cell (PBMC) subsets were first identified by 2-dimensional gating (Figure 1A). Lymphocytes were identified by expression of CD45 and within this gate, major PBMC subsets were identified as follows: CD4Tcon, $CD3^+CD4^+CD25^{neg\text{-}low}FoxP3^-$; CD4Treg, $CD3^+CD4^+CD25^{med\text{-}high}FoxP3^+$; $CD8^+$ T cell; $CD3^+CD8^+$; B cell, $CD3^-CD19^+$; NK cell, $CD3^-CD19^-CD56^+$. We then applied the t-distributed stochastic neighbor embedding algorithm (viSNE) to visualize high-dimensional cytometry data on a 2-dimensional map at single-cell resolution (43) and characterized each of the major PBMC subsets. Figure 1B shows a representative viSNE map of CD4Tregs. Based on expression of CD45RA, CD4Tregs were subdivided into naive ($CD45RA^+$) and memory ($CD45RA^-$) subsets. Helios, a marker of CD4Treg functional activity, was used to further characterize naive and memory CD4Tregs (21, 22). Figure 1, C and D show representative viSNE maps of CD4Tcons and $CD8^+$ T cells, respectively. Based on expression of CD45RA and CD62L, CD4Tcons were clearly divided into 3 subsets (naive Tcon, central memory Tcon, and effector memory Tcon) and $CD8^+$ T cells into 4 subsets (naive, central memory, effector memory, and terminally differentiated effector [TEMRA] $CD8^+$ T cells). Figure 1E shows a representative viSNE map of NK cells. Based on expression of CD56 and CD16, NK cells were

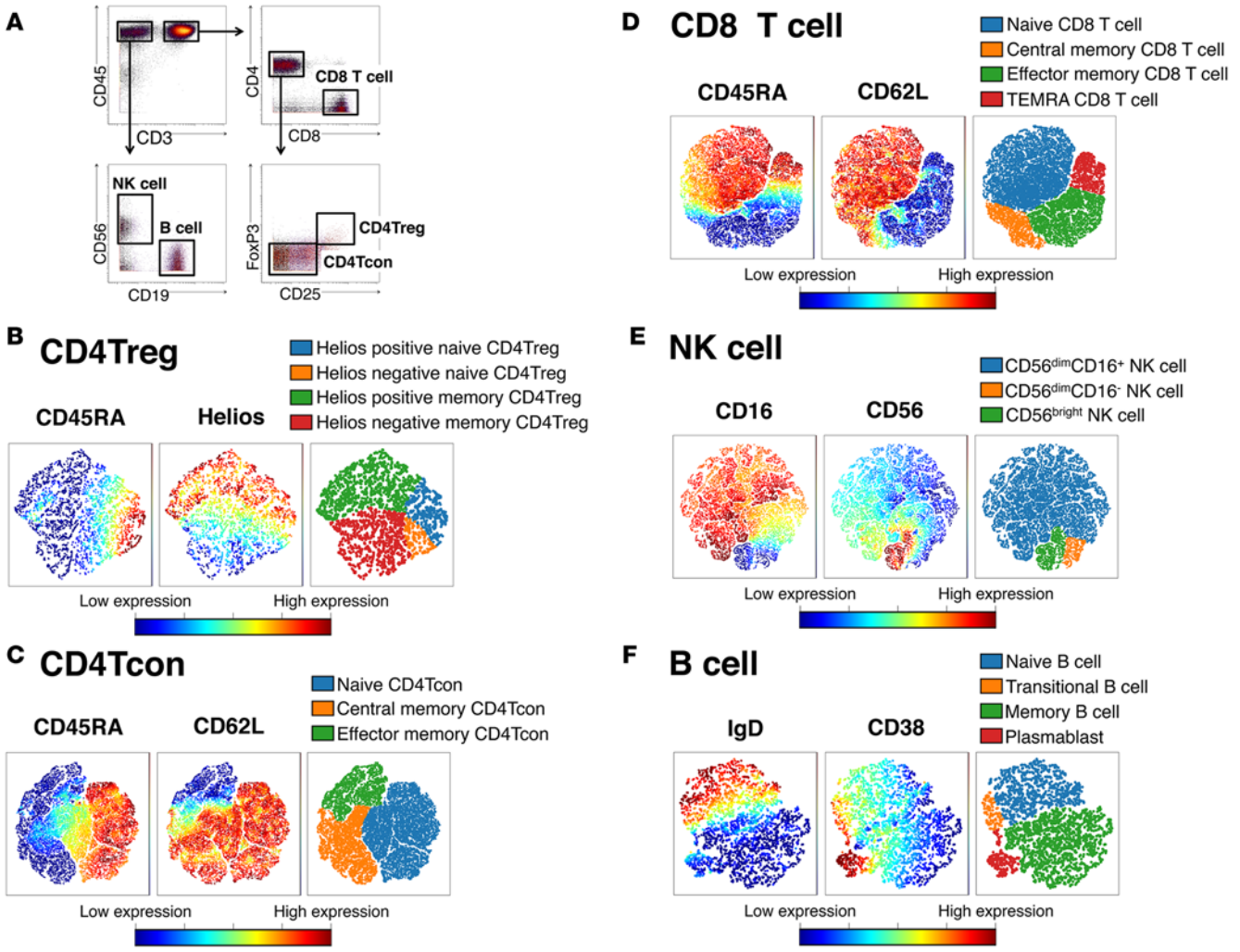

Figure 1. Representative gating and identification of phenotypic lymphocyte subsets in peripheral blood. (**A**) Representative 2-dimensional gating for identification of major lymphocyte subsets in peripheral blood from a healthy donor. (**B**–**F**) viSNE maps of each major lymphocyte subset identified in **A** are shown. Each point in the viSNE map represents an individual cell, and cells are colored according to intensity of expression of the indicated markers. The far-right map in each figure identifies phenotypic subsets based on expression of the indicated markers and the map is color coded for each subset as shown in the color legend.

divided into 3 subsets ($CD56^{dim}CD16^{+}$, $CD56^{dim}CD16^{-}$, and $CD56^{bright}CD16^{-}$ NK cells) (44–46). Lastly, the viSNE map of B cells is shown in Figure 1F. Based on expression of IgD and CD38, B cells were divided into 4 subsets ($IgD^{+}CD38^{lo}$ naive, $IgD^{+}CD38^{++}$ transitional, $IgD^{lo}CD38^{lo}$ memory B cells, and $IgD^{lo}CD38^{++}$ plasmablasts) (5, 47, 48).

Restricted expression of functional proteins in lymphocyte subsets. To further characterize the lymphocyte subsets identified in viSNE, we analyzed expression of several important functional proteins in each major lymphocyte population in normal PBMCs. Figure 2A shows representative expression patterns of these proteins in each T cell population. Notably, these proteins were not uniformly expressed within the major T cell populations. Instead, expression was often segregated within specific subsets. For example, FoxP3 and CD25 expression was highest in $Helios^{+}$ memory CD4Tregs and low-level CD25 expression was restricted to central and effector memory CD4Tcons. CD127 expression was highest in effector memory CD4Tcons, moderate in central memory CD4Tcons, low in naive CD4Tcons and naive $CD8^{+}$ T cells, and very low in TEMRA $CD8^{+}$ T cells. Expression of CD95 was primarily limited to memory subsets but was highest in $Helios^{+}$ memory CD4Tregs. BCL2 was expressed at relatively high levels in most CD4Tregs and CD4Tcons, but within $CD8^{+}$ T cells, BCL2 was only expressed at high levels in naive cells. The MHC class II protein HLA-DR is a known marker of T cell activation. Within the CD4Treg popula-

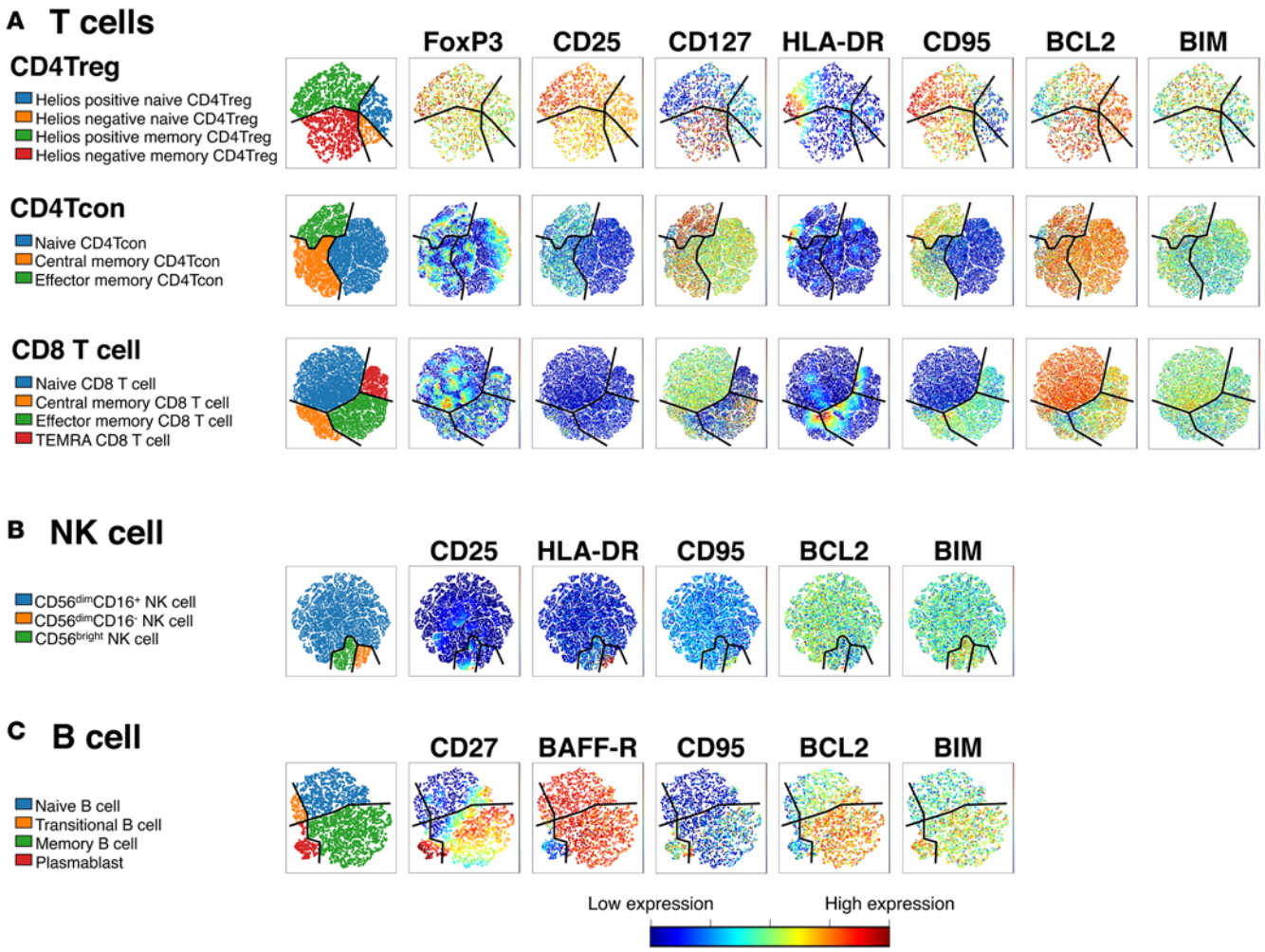

Figure 2. Protein expression in lymphocyte subsets. The viSNE maps for each lymphocyte population are the same as for Figure 1. Each viSNE map shows intensity of expression of the marker indicated for each column. Expression levels of each protein are normalized across all lymphocyte subsets. The far-left map in each row identifies the same phenotypic cell subsets as shown in the color legend and in Figure 1. Expression levels of proteins are shown in (**A**) T cells, (**B**) NK cells, and (**C**) B cells. Data shown are from a single individual and are representative of 5 healthy donor samples.

tion, HLA-DR$^+$ cells were found within the Helios$^+$ memory subset. This same cluster of cells expressed the highest levels of FoxP3, CD25, and CD95 and lowest levels of CD127 and BCL2. Similarly, small clusters of HLA-DR$^+$ cells were evident within CD4Tcons and CD8$^+$ T cells. These activated cells were present primarily in memory subsets and also expressed higher levels of CD95 and lower levels of BCL2 and CD127. Although FoxP3 is primarily expressed in CD4Tregs, small clusters of FoxP3$^+$ cells were also present within CD4Tcons and naive CD8$^+$ T cells.

CD56^{dim}CD16$^-$ and CD56^{bright}CD16$^-$ NK cells are relatively minor NK cell subsets in healthy donors (Figure 2B). CD56^{bright} NK cells express higher levels of CD25, HLA-DR, and BIM than CD56^{dim}CD16$^+$ NK cells (49). CD56^{dim}CD16$^-$ NK cells express low levels of BCL2 and high levels of HLA-DR compared with CD56^{dim}CD16$^+$ NK cells. Figure 2C shows representative expression of key proteins in B cell subsets. As expected, CD27 was expressed at high levels in memory B cells and plasmablasts. B cell–activating factor receptor (BAFF-R) was expressed at high levels in all B cell subsets except for plasmablasts. Expression of CD95 was relatively low in B cells compared with T cells, but its low-level expression in memory B cells and plasmablasts appears to mirror expression of CD27. BCL2 expression was high in memory B cells and low in transitional B cells and plasmablasts. BIM was expressed at higher levels in memory B cells and plasmablasts compared with naive and transitional B cells. As shown by viSNE, each B cell subset expressed a different pattern of these functional molecules, with the most distinctive pattern being in the plasmablast subset that expressed high levels of CD27, BIM, and CD95, with low levels of BCL2 and BAFF-R, suggest-

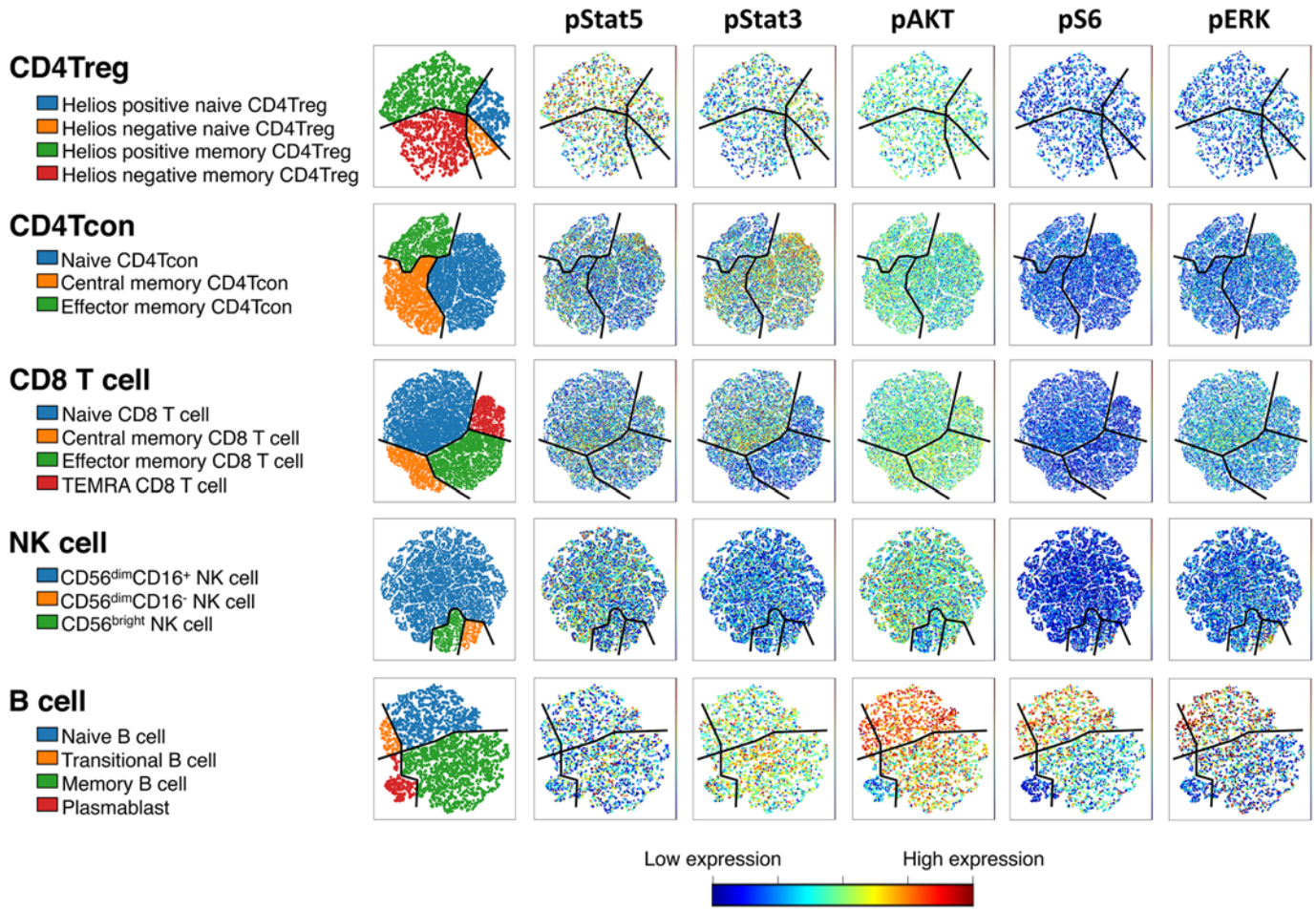

Figure 3. Basal expression of phosphorylated signaling proteins in resting lymphocyte subsets. The viSNE maps for each lymphocyte population are the same as for Figures 1 and 2. Each viSNE map shows intensity of expression of the marker indicated in each column. Expression levels of each phosphoprotein (column) are normalized across lymphocyte subsets. The far-left map in each row identifies the phenotypic cell subsets shown in the color legend. Data shown are from a single individual and are representative of 5 healthy donor samples.

ing that plasmablasts are more highly susceptible to apoptosis than other B cell subsets. Taken together, this comprehensive single-cell platform provides an unprecedented analysis of all major lymphocyte populations and allows the comparison of functional markers within well-defined subsets within each major population.

Constitutive activation of signaling proteins in resting lymphocytes. Our mass cytometry marker panel included 5 antibodies specific for phosphorylated intracellular proteins involved in different cell signaling pathways and viSNE allowed us to assess the baseline levels of each of these phosphoproteins as a measure of constitutive signaling pathway activity in each lymphocyte subset. Figure 3 shows viSNE maps from the same healthy donor shown in Figures 1 and 2. These results are representative of 5 healthy donors. Levels of phospho-STAT5 (p-STAT5) were higher in CD4Tregs than in other T cells at baseline. In CD4Tcons and $CD8^+$ T cells, naive subsets expressed higher levels of p-STAT3 compared with memory subsets. In contrast, p-AKT was expressed at higher levels in memory CD4Tcon and $CD8^+$ T cell subsets compared with naive subsets. Expression of p-S6 and p-ERK was not detected in any resting T cell populations. Within resting NK cells, low levels of p-STAT5 and p-AKT were detected in the major $CD56^{dim}CD16^+$ subset. When compared with T and NK cells, resting B cells exhibited relatively high levels of several signaling proteins including p-STAT3, p-AKT, p-S6, and p-ERK. Expression of p-AKT, p-S6, and p-ERK was highest in naive and transitional B cells and lowest in plasmablasts.

IL-2 concentration-dependent activation of T and NK cell subsets in vitro. Ligand activation of the IL-2 receptor is known to induce phosphorylation of JAK1 and JAK3, leading to phosphorylation of STAT5 (50–52). We previously reported that low concentrations of IL-2 preferentially activate STAT5 in CD4Tregs

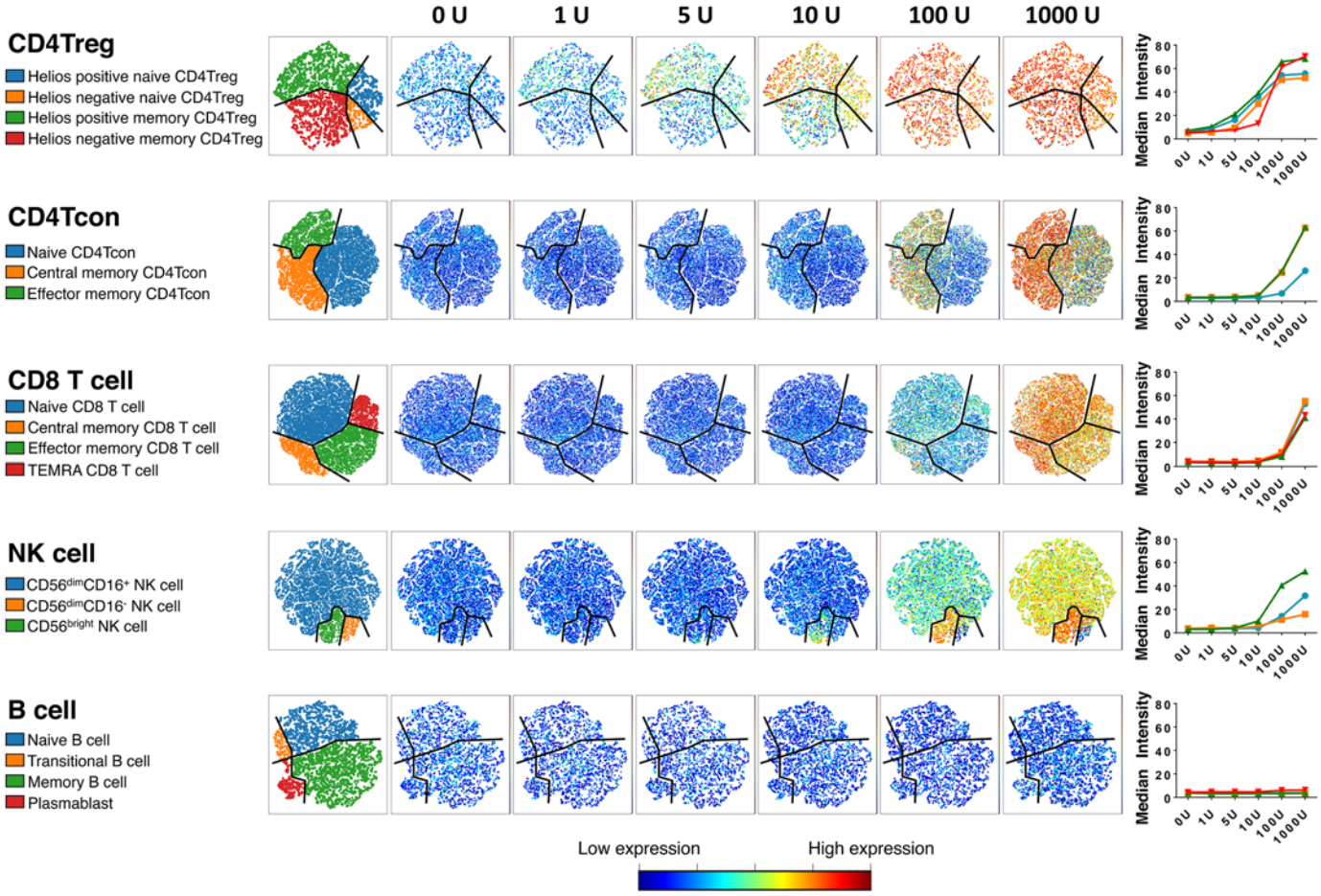

Figure 4. Visualization of p-STAT5 activation after stimulation with varying concentrations of IL-2 in vitro. Peripheral blood mononuclear cells (PBMCs) from healthy donors were stimulated for 15 minutes with varying concentrations of IL-2. Dose-dependent phosphorylation of STAT5 in each lymphocyte subset was monitored by mass cytometry. Each viSNE map shows intensity of expression of p-STAT5 with each indicated concentration of IL-2 (0 to 1,000 IU/ml). Expression levels of p-STAT5 are normalized across all lymphocyte subsets and all concentrations of IL-2. The far-left map in each row identifies the phenotypic cell subsets shown in the color legend. Results in each viSNE map show data from a single representative experiment. Results shown in the far-right graph in each row summarize results (median p-STAT5 expression values) of 5 independent experiments. Median values and ranges for each data point in these graphs are provided in Supplemental Table 2.

compared with CD4Tcons (37). However, to the best of our knowledge the differential effects of IL-2 on various lymphocyte subsets or other signaling pathways have not been examined. To compare the response of each lymphocyte population to IL-2, we stimulated PBMCs from healthy donors with various concentrations of IL-2 for 15 minutes in vitro and simultaneously evaluated the expression of signaling proteins by mass cytometry (Figure 4). As expected, low IL-2 concentrations (1 to 10 IU/ml), preferentially induced p-STAT5 in CD4Tregs. At these low concentrations, p-STAT5 was activated more strongly in Helios$^+$ memory and Helios$^+$ naive CD4Tregs, compared with Helios$^-$ CD4Treg subsets. At high IL-2 concentrations (100 to 1,000 IU/ml), p-STAT5 was activated in all CD4Treg subsets. Within CD4Tcons, high IL-2 concentrations (100 to 1,000 IU/ml) were required to induce p-STAT5 activation and this preferentially occurred in central memory and effector memory subsets. Within CD8$^+$ T cells, very high IL-2 concentrations (≥1,000 IU/ml) were required to induce p-STAT5 and both naive and memory subsets were strongly activated.

Within NK cells, p-STAT5 was detected in the CD56^{bright}CD16$^-$ subset after stimulation with a relatively low IL-2 concentration (10 IU/ml), but the level of activation was lower than in CD4Tregs. At high IL-2 concentrations (100 to 1,000 IU/ml), p-STAT5 was also activated in the major CD56^{dim}CD16$^+$ NK subset, but the level of activation remained higher in the CD56^{bright}CD16$^-$ subset. Very little p-STAT5 activation was detected in the CD56^{dim}CD16$^-$ NK subset. Within B cells, p-STAT5 was not activated at any concentration of IL-2.

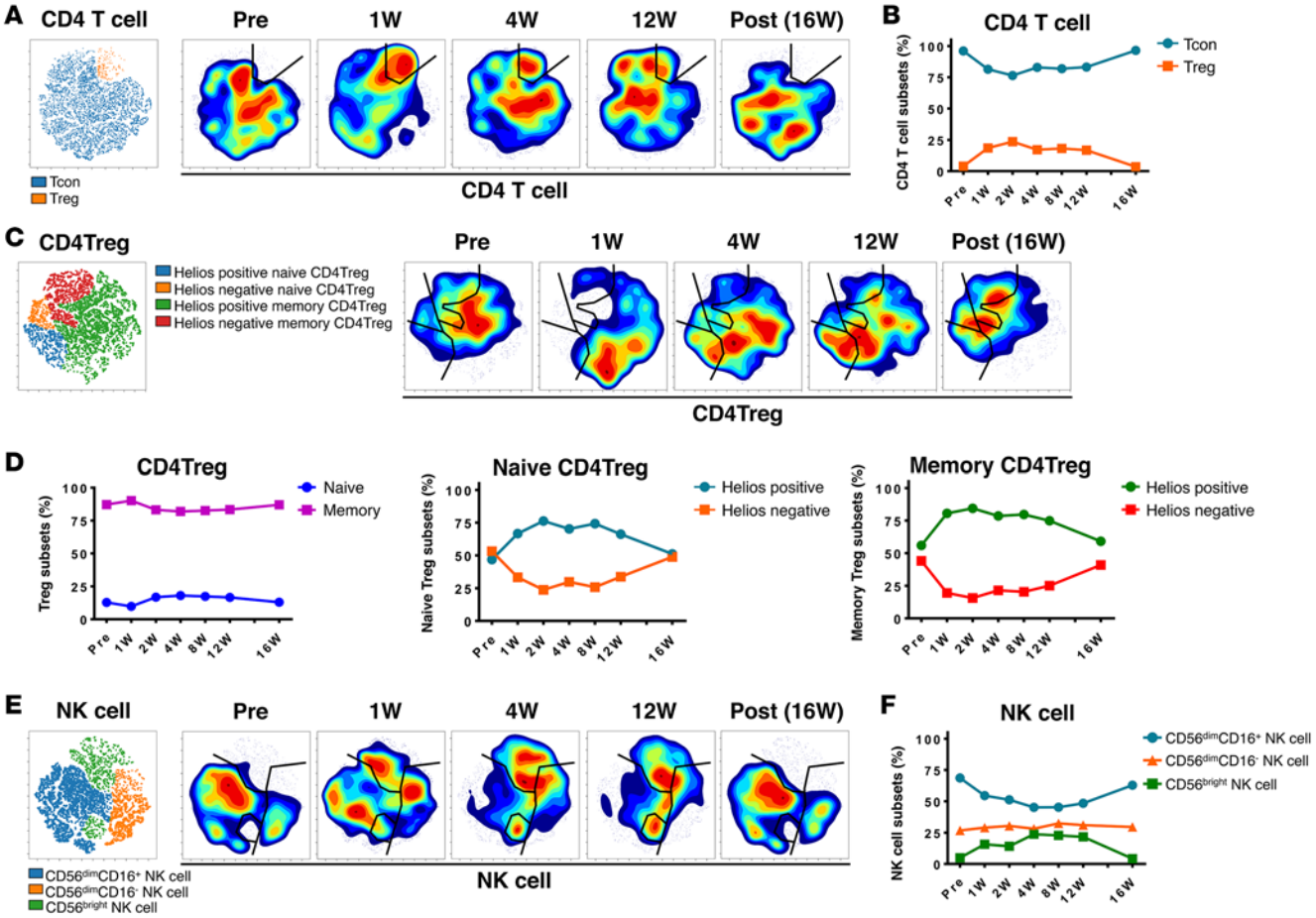

Figure 5. Proportional representation of each lymphocyte subset during low-dose IL-2 therapy in vivo. (**A**) Contour viSNE plots of CD4$^+$ T cells in a representative patient with chronic graft-versus-host disease (GVHD) receiving low-dose IL-2 therapy. The far-left color map identifies CD4$^+$ T cell subsets based on expression of CD25 and FoxP3, and the map is colored to identify conventional CD4$^+$ T cells (CD4Tcons) and CD4$^+$ Tregs (CD4Tregs). The contour maps represent cell density in each region of the map at the indicated time point (in weeks [W]) during IL-2 therapy. (**B**) Summary of CD4$^+$ T cell subset distributions in 14 patients with chronic GVHD receiving low-dose IL-2 therapy, expressed as percentages of total CD4$^+$ T cells, at the indicated time point during therapy. (**C**) Contour viSNE plots of Tregs in a representative patient at the indicated time points during IL-2 therapy. The far-left color map identifies CD4Treg subpopulations that were defined in Figure 1B, and the color for each subpopulation is indicated. (**D**) Summary of CD4Treg subsets in 14 patients receiving daily IL-2 expressed as a percentage of total CD4Tregs (left), naive CD4Tregs (middle), and memory CD4Tregs (right) at the indicated times during therapy. (**E**) Contour viSNE plots of NK cells in a representative patient receiving daily IL-2. The far-left color map next to the contour plots identifies NK subsets that were defined in Figure 1E, and the color for each NK subset is indicated. (**F**) Summary of changes in NK cell subsets in 14 patients receiving daily IL-2 expressed as a percentage of total CD56$^+$ NK cells. Median values and interquartile ranges for each data point in each of these graphs are provided in Supplemental Table 3. Statistical comparisons with pretreatment values are also provided in Supplemental Table 3. Pre, before IL-2 therapy; Post, 4 weeks after stopping IL-2 therapy.

Stimulation with IL-2 induced relatively little activation of other signaling pathways (Supplemental Figures 1–4). IL-2–induced p-STAT3 expression was not detected in any lymphocyte population except CD56^{bright}CD16$^-$ NK cells (Supplemental Figure 1). In control experiments, IL-6 induced p-STAT3 expression in naive T cell subsets (data not shown). IL-2 induced p-AKT and p-ERK expression in CD56^{bright}CD16$^-$ NK cells at a relatively high concentration (100 IU/ml) (Supplemental Figures 2 and 3). At a very high IL-2 concentration (1,000 IU/ml), p-AKT was activated in all NK cell subsets (Supplemental Figure 2). Minimal p-S6 activation was detected in CD56^{bright}CD16$^-$ NK cells at a very high IL-2 concentration (1,000 IU/ml), but IL-2 did not induce p-S6 in any T cell population (Supplemental Figure 4). Activated p-S6 was present at high levels in naive and transitional B cells, but expression was not altered by IL-2 stimulation (Supplemental Figure 4).

Preferential expansion of Helios$^+$ CD4Tregs and CD56^{bright}CD16$^-$ NK cells during low-dose IL-2 therapy in vivo. To examine immunological effects of IL-2 in vivo, we examined PBMCs from 14 patients with refractory chronic GVHD who received daily subcutaneous injections of low-dose IL-2 (1×10^6 IU/m^2/day) for 12

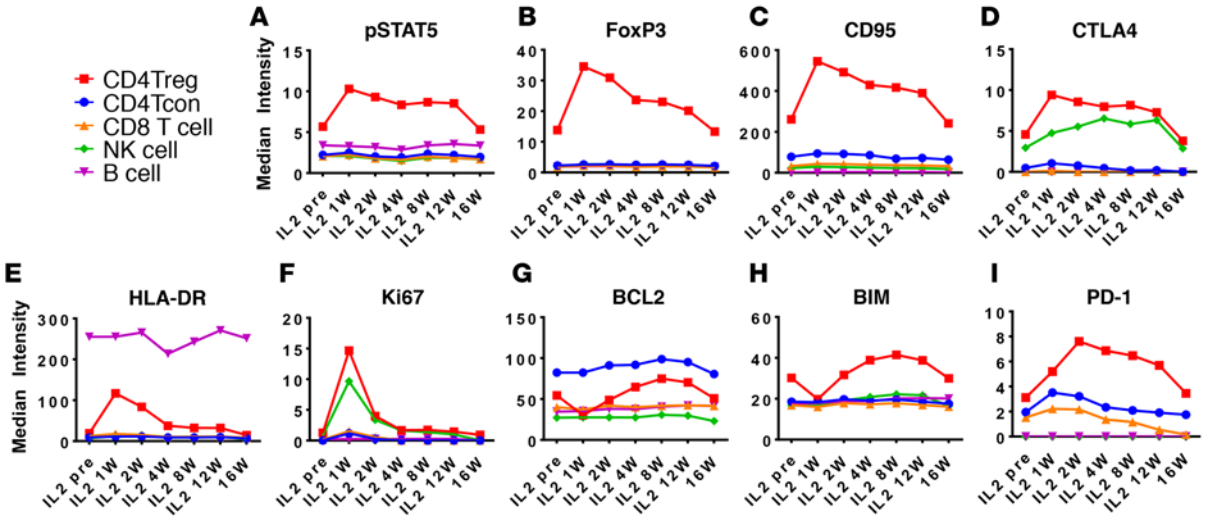

Figure 6. Effect of daily low-dose IL-2 therapy on each major lymphocyte population in vivo. (**A**–**I**) Each graph shows changes in expression of the indicated marker in each lymphocyte population during 12 weeks (12W) of daily low-dose IL-2 therapy and 4 weeks after stopping therapy (16W). Data points represent median values for each indicated marker for 14 patients tested at every time point during therapy. Median values and interquartile ranges for each data point in each of these graphs are provided in Supplemental Table 4. Statistical comparisons with pretreatment values are also provided in Supplemental Table 4.

weeks, followed by a 4-week hiatus. Eight of these patients noted clinical improvement during the initial 12-week treatment period and elected to restart daily IL-2 therapy at the same dose at 16 weeks. Extended daily IL-2 therapy was continued for at least 48 weeks. Clinical characteristics of these patients are summarized in Table 1. We first analyzed changes in the proportion of each lymphocyte population during the first 12 weeks of low-dose IL-2 therapy. Contour plots of viSNE maps focusing on $CD4^+$ T cells from 1 representative patient are shown in Figure 5A. Prior to IL-2 therapy, patients with active chronic GVHD have characteristically low numbers of CD4Tregs. Selective expansion of CD4Tregs was evident after 1 week of treatment. CD4Treg expansion stabilized at 4 weeks and remained elevated at the end of therapy (12 weeks). Four weeks after stopping IL-2 (16 weeks), CD4Treg levels returned to baseline levels. Changes in the proportion of CD4Tregs and CD4Tcons for all 14 patients during low-dose IL-2 are summarized in Figure 5B. The proportion of CD4Tregs peaked 2 weeks after starting low-dose IL-2 and remained elevated during the entire 12-week course of therapy. CD4Treg levels returned to baseline 4 weeks after stopping IL-2.

Applying viSNE to characterize CD4Treg subsets, the expansion of CD4Tregs during low-dose IL-2 therapy was primarily evident in $Helios^+$ subsets (Figure 5C). Changes in CD4Treg subsets from all patients are summarized in Figure 5D. Within both naive and memory CD4Tregs, the proportion of $Helios^+$ cells increased during low-dose IL-2 therapy, while the overall proportions of naive and memory CD4Tregs remained stable. As shown in Figure 5, E and F, selective expansion of $CD56^{bright}CD16^-$ NK cells also occurred during low-dose IL-2 therapy and returned to baseline after IL-2 therapy was stopped. In contrast, no changes were noted in CD4Tcon, $CD8^+$ T cell, or B cell subsets during the 12-week period of low-dose IL-2 therapy (Supplemental Figure 5, A–C).

Effects of low-dose IL-2 therapy on expression of functional proteins. Mass cytometry allowed us to track expression of several important functional proteins in peripheral lymphocytes during low-dose IL-2 therapy. As shown in Figure 6, most changes during low-dose IL-2 therapy occurred in CD4Tregs and $CD56^{bright}CD16^-$ NK cells. Consistent with in vitro studies, p-STAT5 was selectively activated in CD4Tregs, but we did not detect increased expression of p-STAT5 in NK cells. The expression of p-STAT5 in CD4Tregs peaked 1 week after IL-2 therapy began (Figure 6A). CD4Treg p-STAT5 expression decreased after 2 weeks but remained higher than baseline for the duration of therapy ($P = 0.0001$ at 12 weeks). Expression of FoxP3, CD95, CTLA4, and HLA-DR also increased in CD4Tregs, with peak levels occurring 1 week after starting IL-2 (Figure 6, B–E). Although expression of these proteins gradually declined as IL-2 therapy continued, expression levels remained higher than baseline after 12 weeks of daily treatment ($P \leq 0.0002$). As shown in Figure 6F, a dramatic increase in proliferation of CD4Tregs and $CD56^{bright}CD16^-$ NK cells was also observed 1 week after starting IL-2. Proliferation of these cells rapidly returned to baseline levels after 4

Table 1. Clinical characteristics of patients receiving low dose IL-2 (*n* = 14)

	n	(%)		*n*	(%)
Age, median (range)	55	(29–70)	Acute GVHD		
			Grade 2–4	7	(50%)
Patient sex					
Male	8	(57.1)	Time since HSCT		
Female	6	(42.9)	Median days (range)	636.5	(271–1,950)
Diagnosis			Time since onset chronic GVHD		
AML	3	(21.4)	Median days (range)	236.5	(47–1,651)
CLL	3	(21.4)			
ALL	1	(7.1)	Immunosuppressive therapy[A]		
MDS	3	(21.4)	Prednisone		
NHL	4	(28.6)	0 mg	0	(0)
			0 to ≤ 10 mg	4	(28.6)
Conditioning regimen			> 10 mg	10	(71.4)
Myeloablative	7	(50.0)	Tacrolimus		
Nonmyeloablative	7	(50.0)	0 mg	6	(42.9)
			0 to ≤ 1 mg	5	(35.7)
Stem cell source			> 1 mg	3	(21.4)
PBSC	14	(100)	Sirolimus		
Bone marrow	0	(0)	0 mg	12	(85.8)
			0 to ≤ 1 mg	1	(7.1)
Donor type			> 1 mg	1	(7.1)
Matched-related	6	(42.9)	MMF		
Matched-unrelated	7	(50.0)	0 mg	12	(85.8)
Mismatched-unrelated	1	(7.1)	0 to ≤ 500 mg	1	(7.1)
			> 500 mg	1	(7.1)
Acute GVHD prophylaxis					
Sirolimus containing	7	(50.0)			
No sirolimus containing	7	(50.0)			

[A]Immunosuppressive therapy at baseline. ALL, acute lymphoblastic leukemia; AML, acute myeloid leukemia; CLL, chronic lymphocytic leukemia; GVHD, graft-versus-host disease; HSCT, hematopoietic stem cell transplantation; MDS, myelodysplastic syndromes; MMF, mycophenolate mofetil; NHL, non-Hodgkin lymphoma; PBSC, peripheral blood stem cell.

weeks despite continued daily IL-2 therapy. Changes in expression of antiapoptotic BCL2 and proapoptotic BIM proteins were also restricted to CD4Tregs (Figure 6, G and H). Expression of both BCL2 and BIM decreased 1 week after starting IL-2 but recovered to baseline levels at 2 weeks. Subsequently, expression of BCL2 and BIM gradually increased with peak levels occurring 8 weeks after starting IL-2. Expression of PD1 also increased in CD4Tregs during IL-2 therapy, with peak expression occurring 2 weeks after starting treatment (Figure 6I). PD1 was also the only marker in our panel whose expression increased in CD4Tcons and $CD8^+$ T cells during IL-2 therapy. Finally, IL-2 therapy also appeared to induce expression of CTLA4 in the NK cell population.

$Helios^+$ CD4Treg subsets preferentially respond to low-dose IL-2 in vivo. Using viSNE, we were able to further define the effects of IL-2 therapy on CD4Treg subsets in vivo. Figure 7 shows serial viSNE maps of CD4Tregs from a representative patient as well as a summary of changes in protein expression in each CD4Treg subset from all 14 patients. Consistent with results of in vitro stimulation, p-STAT5 was preferentially activated in $Helios^+$ naive and memory CD4Treg subsets during low-dose IL-2 ($Helios^+$ versus $Helios^-$ naive Tregs at 1 week, $P = 0.0002$; $Helios^+$ versus $Helios^-$ memory Tregs at 1 week, $P = 0.0001$) (Figure 7A). Similarly, expression of FoxP3, HLA-DR, Ki67, CD25, and BIM increased primarily in $Helios^+$ CD4Treg subsets (Figure 7, B, E–G, and I). Expression of CD95, CTLA4, and PD-1 increased in $Helios^-$ memory as well as $Helios^+$ CD4Treg subsets. In contrast, BCL2 expression increased preferentially in naive CD4Tregs, including both $Helios^+$ and $Helios^-$ subsets (Figure 7J). The only marker in

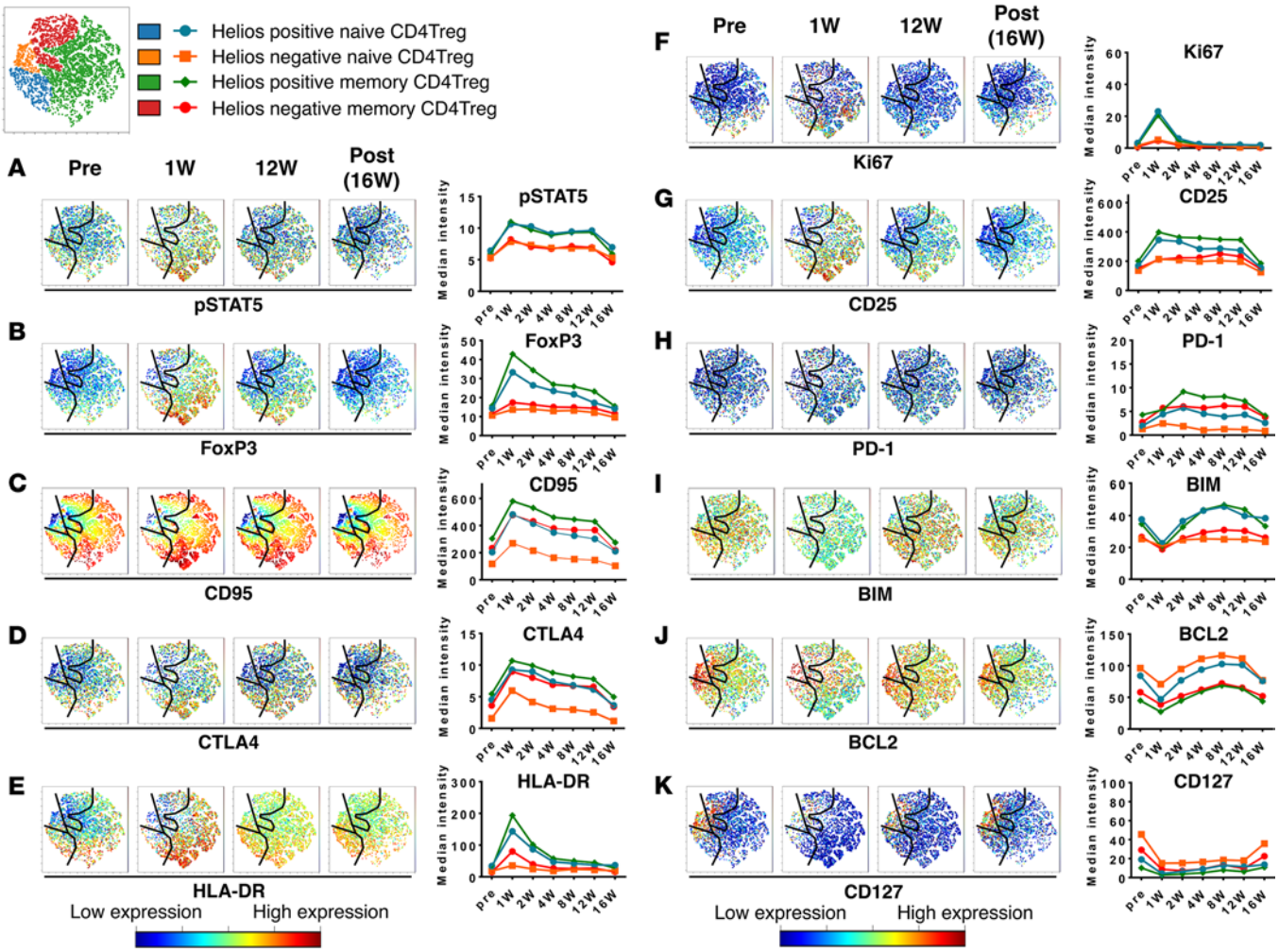

Figure 7. Effects of daily low-dose IL-2 therapy on CD4⁺ Tregs in vivo. (**A**–**K**) Each row shows the viSNE maps of CD4⁺ Tregs (CD4Tregs) in a single representative patient at different time points (in weeks [W]) during daily IL-2 therapy. Different proteins are tracked in each row. In each viSNE map, cells are colored to show intensity of expression of each marker. The location of CD4Treg subsets is color coded at the top of this figure. Median values for expression of each marker in samples from 14 patients at the indicated time points are shown in the graphs to the far right of each row. Median values and interquartile ranges for each data point in each of these graphs are provided in Supplemental Table 5. Statistical comparisons with pretreatment values are also provided in Supplemental Table 5. Pre, before IL-2 therapy; Post, 4 weeks after stopping IL-2 therapy.

our panel with decreased expression in CD4Tregs during IL-2 therapy was CD127 (Figure 7K).

Effects of low-dose IL-2 therapy on NK cell, CD4Tcon, and CD8⁺ T cell subsets. Our analyses of major lymphocyte populations during low-dose IL-2 therapy demonstrated upregulation of Ki67 and CTLA4 in NK cells and increased expression of PD-1 in CD4Tcons and CD8⁺ T cells. More detailed analysis shown in Figure 8A demonstrated that increased proliferation primarily occurred in $CD56^{bright}CD16^{-}$ NK cells, peaking at 1 week after starting IL-2 therapy and then declining. A similar pattern of increased proliferation was also detected in the major population of $CD56^{dim}CD16^{-}$ NK cells, albeit at lower levels. While analysis of the entire NK cell population demonstrated increased expression of CTLA4, more detailed analysis in Figure 8B showed that the $CD56^{bright}CD16^{-}$ NK cell subset constitutively expressed high levels of CTLA4. High-level expression of CTLA4 in this subset did not change during IL-2 therapy, but the selective expansion of $CD56^{bright}CD16^{-}$ NK cells led to the measured increase in CTLA4 expression when the entire NK cell population was considered. Detailed analysis of PD-1 expression in CD4Tcons and CD8⁺ T cell subsets revealed that increased expression of PD-1 was most evident in effector memory CD4Tcons and effector memory CD8⁺ T cells (baseline versus 1 week, $P = 0.0023$ and $P = 0.018$, respectively) (Figure 8, C and D). Although small numbers of FoxP3⁺ cells were detected within CD4Tcon and CD8⁺ T cells, there was

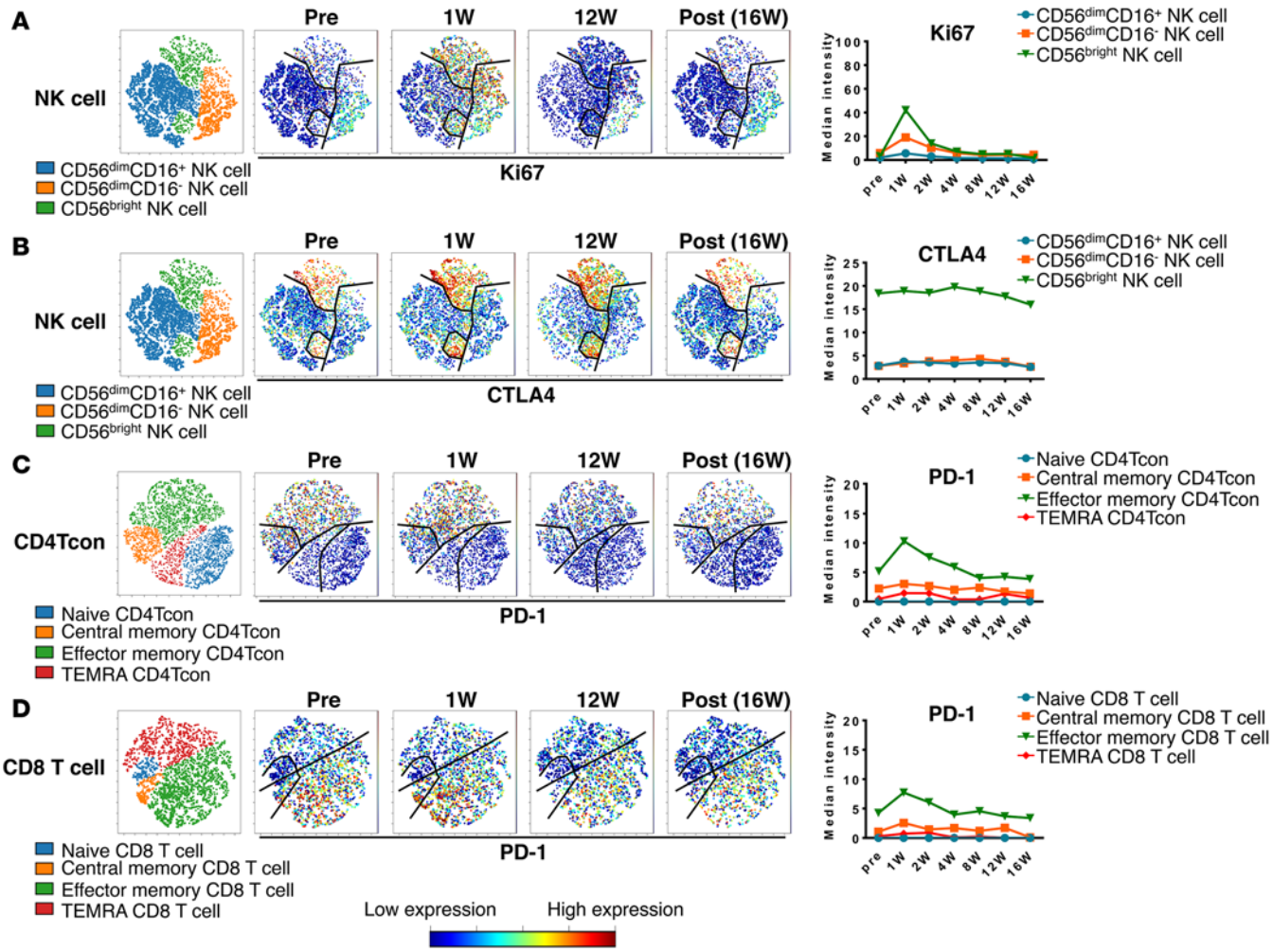

Figure 8. Effects of daily low-dose IL-2 therapy on conventional CD4⁺ T cells, CD8⁺ T cells, and NK cells in vivo. After gating on (**A** and **B**) NK cells, (**C**) conventional CD4⁺ T cells (CD4Tcons), or (**D**) CD8⁺ T cells, each row shows the viSNE maps for a single representative patient at different time points (in weeks [W]) during therapy. Expression of different proteins is tracked in each row. In viSNE maps, cells are colored according to intensity of expression of each indicated marker. The viSNE maps for NK cells (**A** and **B**) are the same as Figure 5E and the maps for CD4Tcons (**C**) and CD8⁺ T cells (**D**) were defined as in Figure 1, C and D, respectively. Median values for expression of each marker in samples from 14 patients at the indicated time points are shown in the graphs to the far right of each row. Median values and interquartile ranges for each data point in each of these graphs are provided in Supplemental Table 6. Statistical comparisons with pretreatment values are also provided in Supplemental Table 6. Pre, before IL-2 therapy; Post, 4 weeks after stopping IL-2 therapy.

no increase in FoxP3 expression in these populations during IL-2 therapy.

Sustained effects of extended low-dose IL-2 therapy on CD4Tregs in vivo. To examine the immunologic effects of extended IL-2 therapy on CD4Tregs, we examined PBMCs from 8 patients who received continuous treatment for at least 48 weeks. The clinical characteristics of these patients are summarized in Supplemental Table 1. In Figure 9, protein expression in CD4Treg subsets measured after 48 weeks of daily low-dose IL-2 is compared with mass cytometry measurements obtained at the end of the initial 12-week IL-2 regimen and 4 weeks after discontinuation of IL-2 (16 weeks). p-STAT5 levels decreased 4 weeks after stopping IL-2, but p-STAT5 levels increased when IL-2 was restarted and remained elevated with extended therapy 48 weeks later (Figure 9A). Similar to the initial course of IL-2 therapy, p-STAT5 was preferentially increased in Helios⁺ CD4Treg subsets during extended therapy. As shown in Figure 9, B–F, expression of other proteins that increased during the initial 12-week treatment period (FoxP3, CD95, CTLA4, CD25, and BCL2) decreased when IL-2 was stopped and increased when IL-2 was restarted. For each of these functionally important proteins, increased expression levels were sustained after 48 weeks of daily IL-2 therapy and their relative expression within different CD4Treg subsets remained stable. For example, expression of FoxP3 and CD25 was preferentially increased in Helios⁺ CD4Treg subsets. Expression of

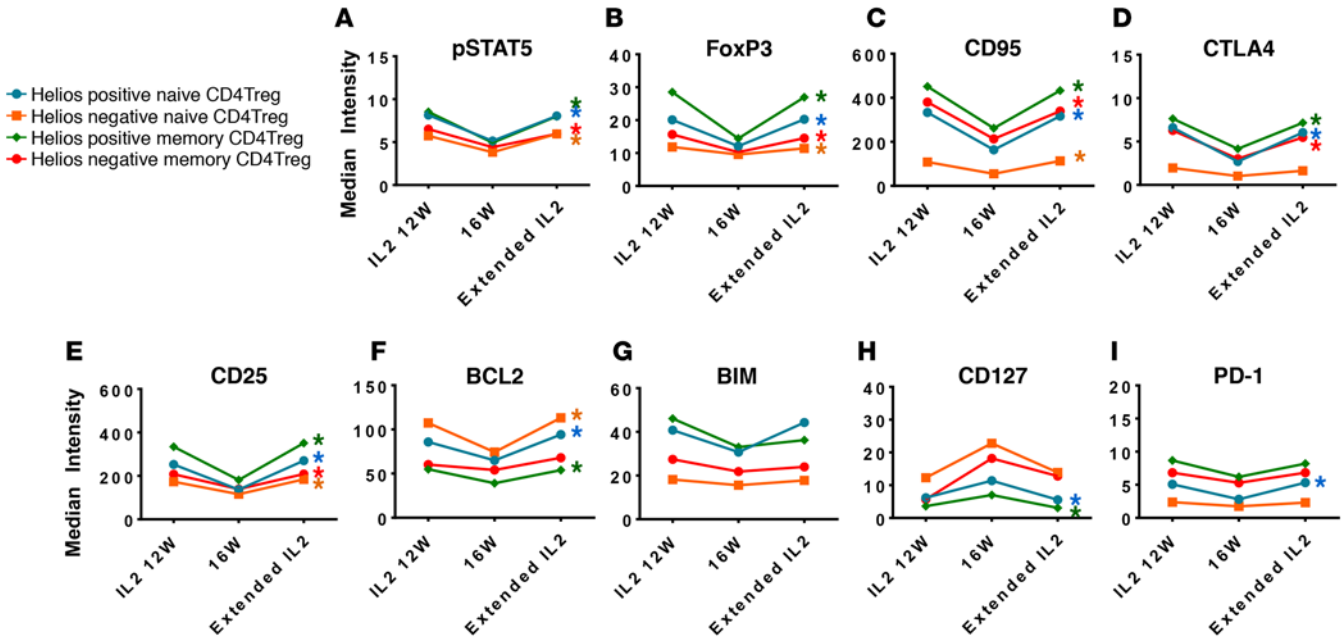

Figure 9. Effect of extended low-dose IL-2 therapy on CD4⁺ Tregs. (**A**–**I**) Individual graphs show changes in expression of each indicated marker in CD4⁺ Treg (CD4Treg) subsets during extended IL-2 therapy. Data points represent median values for each indicated marker from 14 patients at 3 time points (in weeks [W]) during IL-2 therapy: 12W (at completion of initial therapy), 16W (4 weeks after stopping therapy), and 48 weeks after resuming extended therapy. Median values and interquartile ranges for each data point in each of these graphs are provided in Supplemental Table 7. *$P < 0.05$, 16W versus extended period (48W), 2-sided Wilcoxon signed-rank test. All statistical comparisons of 16W and 48W values are provided in Supplemental Table 7.

CD95 and CTLA4 increased more in Helios⁻ memory CD4Treg as well as Helios⁺ naive and memory CD4Treg subsets compared with Helios⁻ naive CD4Tregs. In contrast, BCL2 expression increased preferentially in naive CD4Tregs and changes in BIM expression were not significant (Figure 9G). Although Ki67 expression increased 1 week after starting IL-2, expression was not increased relative to baseline at 12 weeks and there was no significant increase at 48 weeks (data not shown). In contrast with other proteins shown in Figure 9, CD127 (IL-7 receptor) expression in CD4Tregs increased 4 weeks after discontinuation of IL-2 (Figure 9H). CD127 expression decreased during extended therapy, although this change was only statistically significant in Helios⁺ CD4Treg subsets. PD-1 expression did not change significantly during extended IL-2 therapy except for a significant increase in Helios⁺ naive CD4Tregs (Figure 9I).

Discussion

While previous studies have described expression of various functional proteins in different lymphocyte populations, the use of mass cytometry combined with machine learning techniques such as viSNE allowed us to undertake a comprehensive and simultaneous assessment of expression of 33 phenotypic and functional markers in all major lymphocyte subsets at single-cell resolution (43, 53). Application of this marker panel following in vitro stimulation with IL-2 for 15 minutes was used to monitor direct activation of different signaling pathways in each well-defined lymphocyte subset and to correlate signaling activity with expression of functional intracellular proteins as well as surface cytokine receptors. Comparison of a wide range of IL-2 concentrations subsequently identified specific subsets of T cells and NK cells that respond to either physiologic or supraphysiologic concentrations of this important immune cytokine. Finally, examination of serial samples obtained from patients receiving daily low-dose IL-2 therapy for almost 1 year allowed us to compare the results of prolonged administration of exogenous cytokine at physiologic doses with the effects observed following short-term activation in vitro.

The IL-2 receptor is comprised of 3 distinct components, each encoded by different genes and subject to different regulatory mechanisms. IL-2Rβ (CD122) and IL-2Rγ (CD132) are constitutively expressed on all T cells and NK cells and the intracellular domains of these components are responsible for all receptor-mediated signaling activity. However, when expressed individually, IL-2Rβ and IL-2Rγ exhibit low affinity

for IL-2 and when expressed together exhibit moderate binding affinity for IL-2. Constitutive expression of IL-2Rα (CD25) is limited to CD4Tregs and CD56^{bright} NK cells, but expression of IL-2Rα by CD4Tcons and CD8$^+$ T cells is rapidly induced following T cell receptor (TCR) activation. IL-2Rα has no signaling function, but expression of IL-2Rα in conjunction with IL-2Rβ and IL-2Rγ creates a high-affinity trimeric receptor that is capable of responding to low concentrations of IL-2 (54). Our studies demonstrate that constitutive expression of CD25 is restricted to CD4Tregs and CD56^{bright} NK cells and only these populations exhibit signaling activity in response to low concentrations of IL-2. Moreover, within the CD4Treg population, CD25 is expressed at relatively high levels in those cells that express the Helios transcription factor. Both memory and naive CD4Tregs that express Helios can be activated by very low concentrations of IL-2 (1–10 IU/ml). Within CD4Tregs, Helios expression correlates with high expression of FoxP3 and appears to be a marker of the most functionally active or primed subset of CD4Tregs (20, 23). Nevertheless, as IL-2 concentrations increase (10–100 IU/ml), all CD4Tregs are activated. This is consistent with the constitutive expression of high-affinity IL-2Rαβγ on all CD4Tregs. Lacking constitutive expression of CD25, CD4Tcons and CD8$^+$ T cells are not activated at low concentrations of IL-2. However, CD4Tcons and CD8$^+$ T cells express both IL-2Rβ and IL-2Rγ, and IL-2–mediated signaling can be achieved with higher ligand concentrations (100–1,000 IU/ml). Within CD4Tcons, naive cells appear to be relatively resistant to activation, even at very high ligand concentrations. In contrast, all CD8$^+$ T cell subsets are equally activated in response to supraphysiologic concentrations of IL-2. Within all T cell populations, IL-2 signaling appears to be primarily mediated through phosphorylation of STAT5 and we found no activation of STAT3, ERK, AKT, or S6 kinase, even at very high concentrations of IL-2.

Within the NK cell population, cells that express the highest levels of CD56 (CD56^{bright}CD16$^-$) represent a relatively small but discrete subset that exhibits high levels of immune regulatory activity and relatively low levels of cytolytic activity (55). These cells also express CD25 and respond to low concentrations of IL-2 (10 IU/ml). In contrast, the majority of NK cells (CD56^{dim}CD16$^+$) express only IL-2Rβγ and therefore higher concentrations of IL-2 (100–1,000 IU/ml) are required to induce activation of these cells. The small NK cell subset that expresses low levels of CD56 without coexpression of CD16 (CD56^{dim}CD16$^-$) are relatively resistant to high concentrations of IL-2, suggesting that these cells do not express IL-2Rβγ. Like T cells, signaling in NK cells was restricted to STAT5 at low IL-2 concentrations but other pathways (AKT and ERK) were activated at high concentrations of IL-2.

The effects of daily administration of low-dose IL-2 in patients with chronic GVHD closely mirrored the effects of short-term in vitro stimulation of PBMCs with low concentrations of IL-2. Increased proliferation of CD4Tregs was noted 1 week after starting IL-2 treatment and this was associated with selective activation of p-STAT5 in these cells in vivo. STAT3, ERK, AKT, and S6 kinase were not activated in vivo during IL-2 therapy. Activated CD4Tregs rapidly expressed higher levels of FoxP3, CD95, CTLA4, and HLA-DR. CD4Treg expression of PD-1, BCL2, and BIM increased more slowly, with peak expression occurring 2–8 weeks after starting IL-2. Detailed analysis of CD4Treg subsets revealed that these phenotypic changes occurred primarily in Helios$^+$ CD4Tregs. Increased expression of CD95, CTLA4, and PD-1 was also detected in Helios$^-$ memory CD4Tregs, but the expansion of CD4Tregs during 12 weeks of IL-2 therapy was primarily due to selective expansion of Helios$^+$ CD4Tregs, including naive as well as memory CD4Tregs. Proliferation of CD4Tregs and increased expression of HLA-DR returned to baseline levels 2–3 weeks after starting IL-2, but increased expression of other functional markers persisted for the entire 12-week period of daily IL-2 therapy. When IL-2 therapy was stopped, the population of Helios$^+$ CD4Tregs contracted and expression of p-STAT5, FoxP3, CD95, CTLA4, BCL2, BIM, and PD-1 reverted to baseline levels. Taken together, these finding are consistent with murine studies demonstrating that Helios, an Ikaros-family transcription factor, acts to support the functional activity of FoxP3$^+$ Tregs (23). In our studies, expression of Helios specifically identifies human CD4Tregs most capable of responding to low physiologic concentrations of IL-2, regardless of whether these cells have a naive or memory phenotype (20). These cells are also highly dependent on IL-2 and the marked expansion of Helios$^+$ CD4Tregs in vivo was rapidly reversed when IL-2 therapy was stopped. Notably, Helios expression in CD4Tregs did not increase with IL-2 therapy and very few CD4Tcons or CD8$^+$ T cells were found to express Helios.

Consistent with the results of short-term in vitro stimulation, expansion of NK cells during low-dose IL-2 therapy was restricted to the relatively small subset of CD56^{bright}CD16$^-$ NK cells. Although this subset normally represents a small fraction of NK cells in peripheral blood, CD56^{bright}CD16$^-$ NK cells represent the major NK cell population in lymph nodes and tonsils where they reside primarily in parafollicular T cell

zones (55). Lacking expression of CD16, these cells do not mediate antibody-dependent cellular cytotoxicity (ADCC). Expression of cytolytic molecules such as perforin and granzyme is reduced and these cells contain fewer cytolytic granules than $CD56^{dim}CD16^{+}$ NK cells. $CD56^{bright}CD16^{-}$ NK cells typically do not express killer inhibitory receptors (KIRs) but express high levels of inflammatory and immune regulatory cytokines such as interferon-γ (IFN-γ), tumor necrosis factor-α (TNF-α), granulocyte–macrophage colony-stimulating factor (GM-CSF), IL-10, and IL-13. Consistent with these phenotypic characteristics and tissue distribution, $CD56^{bright}CD16^{-}$ NK cells exhibit less cytolytic activity and greater immune regulatory functions than $CD56^{dim}CD16^{+}$ NK cells. However, the cytolytic functions of $CD56^{bright}CD16^{-}$ NK cells increase when these cells are activated (56). $CD56^{bright}CD16^{-}$ NK cells can also differentiate into $CD56^{dim}CD16^{+}$ NK cells under appropriate conditions (55, 57). Our studies demonstrate that the proliferation and expansion of these cells in vivo is very responsive to low concentrations of IL-2, but these conditions in vivo are not sufficient to induce widespread activation and release of regulatory cytokines. Thus, the marked expansion of $CD56^{bright}CD16^{-}$ NK cells in vivo was well tolerated and not associated with toxicities typically associated with cytokine release. Importantly, the expansion of these cells did not lead to exacerbation of chronic GVHD, which improved in more than 50% of patients (30). Although the goal of our clinical studies was to enhance tolerance induction through expansion of CD4Tregs, the ability to selectively enhance the immune regulatory functions of NK cells in vivo with low-dose IL-2 may also have clinical utility. In fact, a recent study found that low levels of $CD56^{bright}$ NK cells were associated with chronic GVHD (58), and the expansion of these cells in response to IL-2 therapy may well have beneficial consequences in patients with chronic GVHD.

While the most dramatic effects of IL-2 therapy were observed within CD4Treg and NK cell populations, we were particularly interested in whether mass cytometry would allow us to detect activated CD4Tcons or $CD8^{+}$ T cells that were responsible for mediating alloimmune responses in patients with active chronic GVHD. Since TCR-activated effector T cells express CD25, these cells would also be expected to respond to low concentrations of IL-2 in vivo. Using activation of STAT5 as a sensitive marker of IL-2 activation, we did not observe expression of p-STAT5 in any subset of CD4Tcons or $CD8^{+}$ T cells during IL-2 therapy. Instead, we found that expression of PD-1 increased in both CD4Tcons and $CD8^{+}$ T cells. This was most evident 1 week after starting IL-2 and coincided with the peak activation of CD4Tregs. Notably, PD-1 expression in CD4Tcons and $CD8^{+}$ T cells was restricted to cells within the effector memory subset. Since this was not associated with increased proliferation or activation of p-STAT5, this likely represents an indirect effect demonstrating the suppressive activity of CD4Tregs.

In our phase 2 clinical trial, patients with active chronic GVHD received daily injections of low-dose IL-2 for 12 weeks followed by a mandatory 4-week period without IL-2 treatment. Patients with clinical improvement of chronic GVHD were eligible to restart IL-2 after the 4-week off-treatment period and could continue daily treatment indefinitely. Although CD4Treg levels reverted to baseline 4 weeks after stopping IL-2, CD4Treg levels increased again when IL-2 was restarted and CD4Treg expansion was maintained for the entire duration of extended IL-2 therapy (30). In the present study, we examined PBMCs from 8 patients who had been on extended IL-2 therapy for 48 weeks. At this late time point, expression of all functional markers of CD4Tregs in our panel was similar to levels that were present at the end of the first 12 weeks of IL-2 therapy. Detailed analysis of CD4Treg subsets after 48 weeks of continuous daily IL-2 treatment revealed that expression of p-STAT5, FoxP3, and CD25 increased most in $Helios^{+}$ CD4Treg subsets, while CD95 and CTLA4 expression increased in $Helios^{-}$ memory CD4Tregs as well as $Helios^{+}$ CD4Tregs. Both CD25 and CTLA4 expression by CD4Tregs are closely linked to the immune regulatory functions of these cells. Through expression of CD25, creating high-affinity IL-2R, CD4Tregs are able to sequester IL-2 from effector T cells and thereby limit the expansion of effector T cells in vivo. Similarly, CTLA4 expressed by CD4Tregs binds to CD80 and CD86 to antagonize costimulation of effector T cells through CD28 (59–61). With prolonged treatment, increased expression of these functional molecules was detected in $Helios^{-}$ as well as $Helios^{+}$ CD4Tregs. Taken together, these changes suggest that prolonged low-dose IL-2 therapy results in significant changes in CD4Treg homeostasis that include all CD4Treg subsets. Although not shown, there was no evidence of activation of CD4Tcons or $CD8^{+}$ T cells with extended IL-2 therapy. Nevertheless, prolonged low-dose IL-2 therapy also resulted in the gradual increase and normalization of CD4Tcon and $CD8^{+}$ T cell counts and restoration of the normal balance between regulatory and effector T cell populations (30).

Recent reports have suggested that low-dose IL-2 may promote immune tolerance in a wide variety of clinical settings in addition to GVHD (32–35, 38, 39, 62, 63). The profound but highly selective immu-

nologic effects of prolonged low-dose IL-2 therapy demonstrated in our studies support further clinical evaluation of this approach in various settings where selective enhancement of CD4Tregs may be needed to restore or maintain immune tolerance.

Methods

Patient characteristics. Laboratory studies were undertaken with blood samples from 14 adult patients with active chronic GVHD at the Dana-Farber Cancer Institute and the Brigham and Women's Hospital, Boston, Massachusetts, USA. Each patient was enrolled in a clinical protocol to define the efficacy of daily low-dose IL-2 for treatment of glucocorticoid-refractory chronic GVHD (30). Recombinant IL-2 (aldesleukin, provided by Prometheus Laboratories) was administered subcutaneously once daily at a dose of 1.0×10^6 IU/m^2 for 12 weeks, followed by a 4-week hiatus. Previous immune-suppressive medications were continued during IL-2 therapy. All study patients completed 12 weeks of treatment. After a 4-week treatment hiatus, 8 patients who achieved a clinical response received extended IL-2 therapy at the same daily dose of IL-2. Clinical characteristics of these patients are summarized in Table 1. The median age of the patients was 55 years (range 29–70). All patients had previously received peripheral blood stem cells (PBSCs) with standard immunosuppressive regimens for GVHD prophylaxis. Fifty percent of patients had a prior history of acute GVHD (grade 2–4). The median time from HSCT to initiation of IL-2 therapy was 636.5 days (range 271–1,950), and the median time from the onset of chronic GVHD to initiation of IL-2 therapy was 236.5 days (range 47–1,651). Ten patients (71.4%) were receiving more than 10 mg of prednisone when IL-2 therapy was started. Similar studies were also undertaken with blood samples from 5 healthy donors (median age 37 years; range 30–55; male/female, 3:2).

Sample preparation. PBMCs were isolated from freshly drawn blood samples by density gradient centrifugation (Ficoll-Paque PLUS; GE Healthcare). Freshly isolated PBMCs from healthy donors were immediately used for in vitro stimulation and antibody staining. PBMCs from patients were washed and cryopreserved in BAMBANKER (Lymphotech) before being analyzed.

Metal-tagged monoclonal antibodies. A panel of 33 metal-tagged monoclonal antibodies was used for analysis of healthy donor and patient PBMCs. A detailed listing of antibodies and corresponding metal tags is provided in Supplemental Table 1. All preconjugated antibodies were purchased from Fluidigm. All other antibodies were purchased in carrier-protein-free PBS and conjugated with the respective metal isotope using the MaxPAR antibody conjugation kit (Fluidigm) according to the manufacturer's recommended protocol. Metal-labeled antibodies were diluted to 0.5 mg/ml in Candor PBS Antibody Stabilization solution (Candor Bioscience GmbH) for long-term storage at 4°C.

Antibody staining for mass cytometry. PBMCs were washed with MaxPar Cell Staining Buffer (Fluidigm) and blocked with Human FcR Blocking Reagent (Miltenyi Biotec) for 10 minutes at room temperature. Cells were then incubated with all antibodies targeting cell surface markers for 30 minutes at room temperature and then washed twice with Cell Staining Buffer. After washing, cells were fixed with Cytofix Fixation Buffer (BD Biosciences) and permeabilized with Phosflow Perm Buffer III (BD Biosciences) following the manufacturer's instructions. Fixed/permeabilized cells were washed twice with Cell Staining Buffer and incubated with all antibodies targeting intracellular antigens for 30 minutes at room temperature. After staining with intracellular antibodies, cells were washed twice with Cell Staining Buffer and incubated with $^{191/193}$Ir DNA intercalator (Fluidigm) following the manufacturer's instructions. Prior to mass cytometry analysis, cells were washed twice with Cell Staining Buffer and twice with MaxPar Water (Fluidigm).

In experiments where PBMCs from healthy donors were stimulated in vitro, fresh samples were processed and stained simultaneously. Patient samples were obtained at different time points after starting IL-2 therapy: baseline pretreatment; 1, 2, 4, 8, and 12 weeks during treatment; 4 weeks after discontinuation of IL-2 (16 weeks); and at 48 weeks in patients receiving extended IL-2 therapy. All samples from an individual patient were thawed and stained simultaneously. Therefore, all samples from a single in vitro stimulation experiment and all samples from an individual patient were processed identically to facilitate comparison across multiple samples.

In vitro stimulation of normal PBMCs with IL-2. To examine IL-2 signaling, freshly isolated PBMCs from healthy donors were stained with surface antibodies prior to in vitro stimulation with IL-2. After washing, cells were incubated in prewarmed PBS supplemented with 2% FBS for 15 minutes at 37°C with 5% CO_2, and then stimulated with different concentrations of IL-2 for 15 minutes at 37°C. To halt signal transduction after stimulation, cells were immediately fixed with Cytofix Fixation Buffer and stained for intracel-

lular markers as described above.

Mass cytometry analysis. Cells were analyzed on a CyTOF 2 mass cytometer (Fluidigm) at an event rate of approximately 500 cells/second. To normalize CyTOF data over different days, EQ Four Element Calibration Beads (Fluidigm) were added in all samples. Resulting data were analyzed with software available through Cytobank (www.cytobank.org). To remove debris and doublets, single cells were gated based on cell length and DNA content as described by Bendall et al. (41). To interpret high-dimensional single-cell data that were produced by mass cytometry, we used a visualization tool based on the viSNE algorithm, which allows visualization of high-dimensional cytometry data on a 2-dimensional map at single-cell resolution and preserve the nonlinearity (43).

Statistics. Data were analyzed with GraphPad Prism version 6.01. The Wilcoxon signed-rank test was used to compare paired samples for continuous variables and expression levels of proteins between subpopulations and between 2 different time points. All tests were 2-sided at the significance level of 0.05 and multiple comparisons were not considered.

Study approval. Patients were enrolled in a phase 2 clinical trial designed to assess the efficacy, safety, and immunologic effects of daily low-dose IL-2 therapy in patients with active chronic GVHD (30). Healthy stem cell donors were enrolled in a tissue-banking protocol for patients with hematologic malignancies and stem cell donors. Protocols were approved by the human subjects protection committee of the Dana-Farber/Harvard Cancer Center. Written informed consent was obtained from each patient and healthy donor before sample collection.

Author contributions

MH designed research studies, conducted experiments, acquired and analyzed data, and wrote the manuscript. TM and KM conducted experiments, acquired and analyzed data, and edited the manuscript. HL, JK, HTK, NP, JW, ACA, SN, CC, VTH, PA, JHA, BRB, JFL, and RJS analyzed data and edited the manuscript. JR designed research studies, analyzed data, and wrote the manuscript.

Acknowledgments

We thank John Daley, Suzan Lazo, and Kristen Leone for excellent assistance with mass cytometry analysis, and Doreen Hearsey and Lauren Gaffny for assistance obtaining clinical blood samples. This work was supported by NIH grants R01CA183559, R01CA183560, R01HL11879, P01CA142106, and P01AI056299, the Jock and Bunny Adams Education and Research Endowment, and the Ted and Eileen Pasquarello Research Fund

Address correspondence to: Jerome Ritz, Dana-Farber Cancer Institute, 450 Brookline Avenue, M530, Boston, Massachusetts 02215, USA. Phone: 617.632.3465; E-mail: Jerome_Ritz@dfci.harvard.edu.

1. Martin PJ, et al. Life expectancy in patients surviving more than 5 years after hematopoietic cell transplantation. *J Clin Oncol*. 2010;28(6):1011–1016.
2. Wingard JR, et al. Long-term survival and late deaths after allogeneic hematopoietic cell transplantation. *J Clin Oncol*. 2011;29(16):2230–2239.
3. Socié G, Ritz J. Current issues in chronic graft-versus-host disease. *Blood*. 2014;124(3):374–384.
4. Blazar BR, Murphy WJ, Abedi M. Advances in graft-versus-host disease biology and therapy. *Nat Rev Immunol*. 2012;12(6):443–458.
5. Sarantopoulos S, et al. Recovery of B-cell homeostasis after rituximab in chronic graft-versus-host disease. *Blood*. 2011;117(7):2275–2283.
6. Cutler C, et al. Rituximab for steroid-refractory chronic graft-versus-host disease. *Blood*. 2006;108(2):756–762.
7. Sakaguchi S, Yamaguchi T, Nomura T, Ono M. Regulatory T cells and immune tolerance. *Cell*. 2008;133(5):775–787.
8. Wing K, Sakaguchi S. Regulatory T cells exert checks and balances on self tolerance and autoimmunity. *Nat Immunol*. 2010;11(1):7–13.
9. Alho AC, et al. Unbalanced recovery of regulatory and effector T cells after allogeneic stem cell transplantation contributes to chronic GVHD. *Blood*. 2016;127(5):646–657.
10. Matsuoka K, et al. Altered regulatory T cell homeostasis in patients with $CD4^+$ lymphopenia following allogeneic hematopoietic stem cell transplantation. *J Clin Invest*. 2010;120(5):1479–1493.
11. Murase K, et al. Increased mitochondrial apoptotic priming of human regulatory T cells after allogeneic hematopoietic stem cell transplantation. *Haematologica*. 2014;99(9):1499–1508.
12. Kawano Y, et al. Low telomerase activity in $CD4^+$ regulatory T cells in patients with severe chronic GVHD after hematopoietic stem cell transplantation. *Blood*. 2011;118(18):5021–5030.
13. Takahata Y, et al. $CD25^+CD4^+$ T cells in human cord blood: an immunoregulatory subset with naive phenotype and specific

expression of forkhead box p3 (Foxp3) gene. *Exp Hematol*. 2004;32(7):622–629.
14. Valmori D, Merlo A, Souleimanian NE, Hesdorffer CS, Ayyoub M. A peripheral circulating compartment of natural naive CD4 Tregs. *J Clin Invest*. 2005;115(7):1953–1962.
15. Baecher-Allan C, Wolf E, Hafler DA. MHC class II expression identifies functionally distinct human regulatory T cells. *J Immunol*. 2006;176(8):4622–4631.
16. Miyara M, et al. Functional delineation and differentiation dynamics of human $CD4^+$ T cells expressing the FoxP3 transcription factor. *Immunity*. 2009;30(6):899–911.
17. Bruno L, et al. Runx proteins regulate Foxp3 expression. *J Exp Med*. 2009;206(11):2329–2337.
18. Thornton AM, et al. Expression of Helios, an Ikaros transcription factor family member, differentiates thymic-derived from peripherally induced $Foxp3^+$ T regulatory cells. *J Immunol*. 2010;184(7):3433–3441.
19. Gottschalk RA, Corse E, Allison JP. Expression of Helios in peripherally induced $Foxp3^+$ regulatory T cells. *J Immunol*. 2012;188(3):976–980.
20. Himmel ME, MacDonald KG, Garcia RV, Steiner TS, Levings MK. $Helios^+$ and $Helios^-$ cells coexist within the natural $FOXP3^+$ T regulatory cell subset in humans. *J Immunol*. 2013;190(5):2001–2008.
21. Akimova T, Beier UH, Wang L, Levine MH, Hancock WW. Helios expression is a marker of T cell activation and proliferation. *PLoS One*. 2011;6(8):e24226.
22. Zabransky DJ, et al. Phenotypic and functional properties of $Helios^+$ regulatory T cells. *PLoS One*. 2012;7(3):e34547.
23. Kim HJ, et al. Stable inhibitory activity of regulatory T cells requires the transcription factor Helios. *Science*. 2015;350(6258):334–339.
24. Yu A, Malek TR. Selective availability of IL-2 is a major determinant controlling the production of $CD4^+CD25^+Foxp3^+$ T regulatory cells. *J Immunol*. 2006;177(8):5115–5121.
25. Boyman O, Sprent J. The role of interleukin-2 during homeostasis and activation of the immune system. *Nat Rev Immunol*. 2012;12(3):180–190.
26. Weist BM, Kurd N, Boussier J, Chan SW, Robey EA. Thymic regulatory T cell niche size is dictated by limiting IL-2 from antigen-bearing dendritic cells and feedback competition. *Nat Immunol*. 2015;16(6):635–641.
27. Liao W, Lin JX, Leonard WJ. Interleukin-2 at the crossroads of effector responses, tolerance, and immunotherapy. *Immunity*. 2013;38(1):13–25.
28. Amado IF, et al. IL-2 coordinates IL-2-producing and regulatory T cell interplay. *J Exp Med*. 2013;210(12):2707–2720.
29. Koreth J, et al. Interleukin-2 and regulatory T cells in graft-versus-host disease. *N Engl J Med*. 2011;365(22):2055–2066.
30. Koreth J, et al. Efficacy, durability, and response predictors of low-dose interleukin-2 therapy for chronic graft-versus-host disease. *Blood*. 2016;128(1):130–137.
31. Ito S, et al. Ultra-low dose interleukin-2 promotes immune-modulating function of regulatory T cells and natural killer cells in healthy volunteers. *Mol Ther*. 2014;22(7):1388–1395.
32. Saadoun D, et al. Regulatory T-cell responses to low-dose interleukin-2 in HCV-induced vasculitis. *N Engl J Med*. 2011;365(22):2067–2077.
33. Hartemann A, et al. Low-dose interleukin 2 in patients with type 1 diabetes: a phase 1/2 randomised, double-blind, placebo-controlled trial. *Lancet Diabetes Endocrinol*. 2013;1(4):295–305.
34. Kennedy-Nasser AA, et al. Ultra low-dose IL-2 for GVHD prophylaxis after allogeneic hematopoietic stem cell transplantation mediates expansion of regulatory T cells without diminishing antiviral and antileukemic activity. *Clin Cancer Res*. 2014;20(8):2215–2225.
35. Castela E, et al. Effects of low-dose recombinant interleukin 2 to promote T-regulatory cells in alopecia areata. *JAMA Dermatol*. 2014;150(7):748–751.
36. von Spee-Mayer C, et al. Low-dose interleukin-2 selectively corrects regulatory T cell defects in patients with systemic lupus erythematosus. *Ann Rheum Dis*. 2016;75(7):1407–1415.
37. Matsuoka K, et al. Low-dose interleukin-2 therapy restores regulatory T cell homeostasis in patients with chronic graft-versus-host disease. *Sci Transl Med*. 2013;5(179):179ra43.
38. Rosenzwajg M, et al. Low-dose interleukin-2 fosters a dose-dependent regulatory T cell tuned milieu in T1D patients. *J Autoimmun*. 2015;58:48–58.
39. Yu A, et al. Selective IL-2 responsiveness of regulatory T cells through multiple intrinsic mechanisms supports the use of low-dose IL-2 therapy in type 1 diabetes. *Diabetes*. 2015;64(6):2172–2183.
40. Bandura DR, et al. Mass cytometry: technique for real time single cell multitarget immunoassay based on inductively coupled plasma time-of-flight mass spectrometry. *Anal Chem*. 2009;81(16):6813–6822.
41. Bendall SC, et al. Single-cell mass cytometry of differential immune and drug responses across a human hematopoietic continuum. *Science*. 2011;332(6030):687–696.
42. Newell EW, Sigal N, Bendall SC, Nolan GP, Davis MM. Cytometry by time-of-flight shows combinatorial cytokine expression and virus-specific cell niches within a continuum of $CD8^+$ T cell phenotypes. *Immunity*. 2012;36(1):142–152.
43. Amir el-AD, et al. viSNE enables visualization of high dimensional single-cell data and reveals phenotypic heterogeneity of leukemia. *Nat Biotechnol*. 2013;31(6):545–552.
44. Cooper MA, Fehniger TA, Caligiuri MA. The biology of human natural killer-cell subsets. *Trends Immunol*. 2001;22(11):633–640.
45. Dulphy N, et al. An unusual CD56(bright) CD16(low) NK cell subset dominates the early posttransplant period following HLA-matched hematopoietic stem cell transplantation. *J Immunol*. 2008;181(3):2227–2237.
46. Béziat V, et al. $CD56^{bright}CD16^+$ NK cells: a functional intermediate stage of NK cell differentiation. *J Immunol*. 2011;186(12):6753–6761.
47. Bohnhorst JØ, Bjørgan MB, Thoen JE, Natvig JB, Thompson KM. Bm1-Bm5 classification of peripheral blood B cells reveals circulating germinal center founder cells in healthy individuals and disturbance in the B cell subpopulations in patients with primary Sjögren's syndrome. *J Immunol*. 2001;167(7):3610–3618.
48. Sims GP, Ettinger R, Shirota Y, Yarboro CH, Illei GG, Lipsky PE. Identification and characterization of circulating human transitional B cells. *Blood*. 2005;105(11):4390–4398.

49. Caligiuri MA, Zmuidzinas A, Manley TJ, Levine H, Smith KA, Ritz J. Functional consequences of interleukin 2 receptor expression on resting human lymphocytes. Identification of a novel natural killer cell subset with high affinity receptors. *J Exp Med*. 1990;171(5):1509–1526.
50. Lin JX, et al. The role of shared receptor motifs and common Stat proteins in the generation of cytokine pleiotropy and redundancy by IL-2, IL-4, IL-7, IL-13, and IL-15. *Immunity*. 1995;2(4):331–339.
51. Nakajima H, et al. An indirect effect of Stat5a in IL-2-induced proliferation: a critical role for Stat5a in IL-2-mediated IL-2 receptor alpha chain induction. *Immunity*. 1997;7(5):691–701.
52. Imada K, et al. Stat5b is essential for natural killer cell-mediated proliferation and cytolytic activity. *J Exp Med*. 1998;188(11):2067–2074.
53. Becher B, et al. High-dimensional analysis of the murine myeloid cell system. *Nat Immunol*. 2014;15(12):1181–1189.
54. Stauber DJ, Debler EW, Horton PA, Smith KA, Wilson IA. Crystal structure of the IL-2 signaling complex: paradigm for a heterotrimeric cytokine receptor. *Proc Natl Acad Sci USA*. 2006;103(8):2788–2793.
55. Caligiuri MA. Human natural killer cells. *Blood*. 2008;112(3):461–469.
56. Fehniger TA, et al. CD56bright natural killer cells are present in human lymph nodes and are activated by T cell-derived IL-2: a potential new link between adaptive and innate immunity. *Blood*. 2003;101(8):3052–3057.
57. Vivier E, Tomasello E, Baratin M, Walzer T, Ugolini S. Functions of natural killer cells. *Nat Immunol*. 2008;9(5):503–510.
58. Kariminia A, et al. Heterogeneity of chronic graft-versus-host disease biomarkers: association with CXCL10 and CXCR3$^+$ NK cells. *Blood*. 2016;127(24):3082–3091.
59. Wing K, et al. CTLA-4 control over Foxp3$^+$ regulatory T cell function. *Science*. 2008;322(5899):271–275.
60. Zhang R, Huynh A, Whitcher G, Chang J, Maltzman JS, Turka LA. An obligate cell-intrinsic function for CD28 in Tregs. *J Clin Invest*. 2013;123(2):580–593.
61. Zheng Y, et al. Acquisition of suppressive function by activated human CD4$^+$ CD25$^-$ T cells is associated with the expression of CTLA-4 not FoxP3. *J Immunol*. 2008;181(3):1683–1691.
62. Humrich JY, et al. Rapid induction of clinical remission by low-dose interleukin-2 in a patient with refractory SLE. *Ann Rheum Dis*. 2015;74(4):791–792.
63. He J, et al. Low-dose interleukin-2 treatment selectively modulates CD4(+) T cell subsets in patients with systemic lupus erythematosus. *Nat Med*. 2016;22(9):991–993.